Characterizing Gas-Collection Volumes with Acoustic and Microwave Resonances

Jodie G. Pope[a], Keith A. Gillis[a], Michael R Moldover[a], James B. Mehl[b], and Eric Harman[c].

[a] *Fluid Metrology Group, NIST, Gathersburg, MD 20899, USA*

[b] *36 Zunuqua Trail, P.O. Box 307, Orcas, WA 98280-0307, USA*

[c] *Colorado Engineering Experiment Station, Inc (CEESI), USA*

Abstract

We characterized a 1.8 m^3, nearly-spherical, steel shell at pressures up to 7 MPa for use as a gas flow standard. For pressure, volume, temperature, and time measurements, the shell's cavity will collect gas; for blow-down measurements, the shell will be a gas source. We measured the cavity's microwave resonance frequencies f_{micro} to determine its pressure- and temperature-dependent volume: $V_{micro}(P, T) = 1.84740\ m^3 \times [1 + \alpha(T–295\ K) + \kappa P]$ with a fractional uncertainty of 0.011 % at a 68 % confidence level. The coefficients α and κ were consistent with the dimensions and properties of the steel shell. The microwave-determined volume V_{micro} was consistent, within combined uncertainties, with V_{gas} the volume determined by a gas expansion method: $V_{micro}/V_{gas} - 1 = (2 \pm 14)\times10^{-5}$. When the shell was filled with gas, measurements of its acoustic resonance frequencies f_{acoust} and of the pressure quickly and accurately determined the mass of the gas in the shell, even when temperature gradients persisted. [K. A. Gillis *et al*. *Metrologia*, **52**, 337 (2015)] After raising the nitrogen pressure in the shell from 0.1 MPa to 7.0 MPa in 45 minutes, the top of the shell was ≈20 °C warmer than the bottom of the shell. Despite this large thermal gradient, the mass M_{acoust} of gas determined from acoustic resonance frequencies settled to within 0.01 % of its final value after 5 h. Following a smaller pressure change of 0.3 MPa, the top-to-bottom temperature difference was 1.5 °C and M_{acoust} settled to its final value in just 0.5 h.

Nomenclature

a	Inner radius
α	Thermal expansion coefficient
β_a	Acoustic virial coefficients
B	Density virial coefficients
c_0	Speed of light in vacuum
D_T	Thermal diffusivity of gas in BBB
f_{micro}	Microwave resonance frequency
$\left\langle f_{ln}^{\sigma} \right\rangle$	Average frequency of a microwave multiplet.
f_{acoust}	Acoustic resonance frequency
γ_0	$\equiv C_p/C_V$, zero-density ratio of the constant-volume specific heat to the constant-pressure specific heat.
j_0	Zeroth order spherical Bessel function
κ	Pressure expansion coefficient
M_{acoust}	Mass determined from f_{acoust}
M_{BBB}	Mass of gas in the BBB
M_∞	Equilibrium mass in BBB at time infinity
M_{grav}	Mass of gas determined by a weighing technique
n_g	Refractive index of a gas
P	Pressure

1. Introduction

During 2016, the value of natural gas metered in pipelines in the United States was approximately $90 billion. To ensure equity at each transfer of custody, accurate metering is required, both in the US and international markets. NIST calibrates natural gas flow meters and has an ongoing research program to improve the accuracy these calibrations [1]. At present, NIST traces the calibration of pipeline-scale natural gas flowmeters to NIST's primary gas flow standard that uses the pressure, volume, temperature, and time (*PVTt*) technique [2]. This primary standard relies on a well-characterized, carefully-thermostated [$u(T)$ = 6 mK][1], 0.67 m^3 collection vessel that operates at pressures up to 0.15 MPa. The primary standard is used to calibrate, one at a time, 21 critical flow venturis (CFVs), each 5.2 mm in diameter. The 21 CFVs are used in parallel to calibrate several 25 mm-diameter CFVs, one at a time [3]. This use of 21 CFVs in parallel is the first of 6 stages of scale-up that uses both CFVs and

[1] Unless otherwise stated, all uncertainties are one standard uncertainty corresponding to 68 % confidence level.

Nomenclature (continued)

ρ	Gas density
$\varphi_i(\mathrm{r})$	Acoustic velocity potential of a standing wave as a function of radius in a sphere.
T	Temperature
$\langle T\rangle_{\mathrm{sh}}$	Average shell thermometer readings
$\langle T\rangle_V$	Volume average temperature
$\langle T\rangle_\varphi$	Acoustic mode-dependent average temperature
τ	Time required for a changing quantity to reach 63.2 % of its new value.
u	Standard uncertainty
u_{r}	Relative standard uncertainty such that $u_{\mathrm{r}}(x) = u(x)/x$
V_{micro}	Volume of BBB determined by microwave resonance frequencies
V_{acoust}	Volume of BBB determined by acoustic resonance frequencies
V_{gas}	Volume of BBB determined by gas expansion
V_{addenda}	Volume of ports and fittings on BBB that are not detected by the long-wavelength microwaves and sound waves.
$V_{\mathrm{inventory}}$	Volume of the connecting plumbing between the BBB and the reference volume for the gas expansion measurement.
V_{ref}	Volume of the reference used in the gas expansion measurement.
w	Speed of sound
$\langle w\rangle$	Average speed of sound
x_{w}	Mole fraction of water in a gas
ξ_{ln}^{σ}	Exactly-known microwave eigenvalue of a spherical cavity, σ = TM or TE
Z	$= P/(\rho RT)$, compressibility factor.
z_{acoust}	Exactly-known acoustic eigenvalue of a spherical cavity

turbine meters. The scale-up begins with flows of ≈10 g/s and ends with flows encountered in large natural gas pipelines: ≈500 kg/s at pressures near 7 MPa. Each stage of scale-up adds cost and uncertainty to the calibration of large meters. The purpose of this work is to reduce the number of stages in the traceability chain by starting with a novel, primary gas-flow standard that operates at higher pressures and flow rates than NIST's present primary standard.

In this paper, we characterize a large volume (1.8 m^3) enclosed by a nearly-spherical, steel shell. This volume may be used at pressures up to 7 MPa as either a gas source or as a gas collector during calibrations of CFVs and other meters. Informally, we call the steel shell the Big Blue Ball (BBB). We used microwave resonance frequencies f_{micro} to determine the $V_{\mathrm{micro}}(P, T)$ of the BBB, where V, T, P are the volume, temperature and pressure, respectively. A summary of the microwave results is:

$$\begin{aligned} V_{\mathrm{micro}}(P,T) &= 1.84740\ \mathrm{m}^3(1\pm 1.1\times 10^{-4})[1+\alpha(T-295\mathrm{K})+\kappa P), \\ \alpha/\mathrm{K} &= 5.24\times 10^{-5}(1\pm 0.081), \\ \kappa/\mathrm{MPa} &= 1.790\times 10^{-4}(1\pm 0.013). \end{aligned} \quad (1)$$

Figure 1 displays $V_{\mathrm{micro}}(P, T)$ and the deviations from Eq. (1). We also used a gas expansion technique to independently measure the volume of the BBB, V_{gas}(0.1 MPa, 295 K). As shown in Fig. 1(a), the two techniques agreed within combined uncertainties: $V_{\mathrm{micro}}/V_{\mathrm{gas}} - 1 = (2 \pm 14)\times 10^{-5}$.

In addition to measuring $V_{\mathrm{micro}}(P, T)$ we determined M_{BBB}, the mass of the gas in the BBB, by measuring acoustic resonance frequencies f_{acoust} and the pressure. First, we discuss determining M_{BBB} when the BBB and the gas within it are in thermal equilibrium; then we discuss the effects of temperature gradients.

We determined the speed of sound $w(P, T)$ in the gas using the relation

$$w = f_{\mathrm{acoust}}\left(6\pi^2 V_{\mathrm{micro}}\right)^{1/3} / z_{\mathrm{acoust}}\ , \quad (2)$$

where z_{acoust} is an exactly-known eigenvalue of a spherical cavity [4]. With w known, we determined the gas density $\rho(P, w)$ using tables that we generated using the computer package REFPROP [5]. Finally, we determined the mass of the gas in the BBB from the product

$$M_{\mathrm{acoust}} = V_{\mathrm{micro}}\rho(P,w)\,. \quad (3)$$

To provide insight into the sensitivity of M_{acoust} to our measurements and to the REFPROP-generated tables, we follow Gillis *et al*. [6] in using the exact (but truncated) virial expansions of $P(\rho, T)$ and $w(\rho, T)$ to calculate $\rho(P, w)$. The result is:

$$M_{\text{acoust}} = \frac{\gamma_0 P V_{\text{micro}}}{w^2}\left[1 + (\beta_a - B)\frac{P}{RT} + \ldots\right] . \qquad (4)$$

In Eq. (4), $\gamma_0 \equiv C_P/C_V$ is the zero-density ratio of the constant-pressure specific heat to the constant-volume specific heat, and β_a and B are the acoustic and the density virial coefficients, respectively. In Eq. (4), the real-gas term, $(\beta_a - B)P/(RT)$ is 0.073 for nitrogen at 295 K and 7 MPa, and the sum of all the terms in the brackets is 1.097. The uncertainty of M_{acoust} is the combined uncertainties of the measured quantity $\gamma_0 P V_{\text{micro}}/w^2$ and the quantity in the brackets obtained from the equation of state. For nitrogen, argon, methane, and several other gases, the relative uncertainty of $u_r(\rho(P, w)) \le 3\times10^{-4}$ for $P \le 7$ MPa and $T \approx 20$ °C [5].

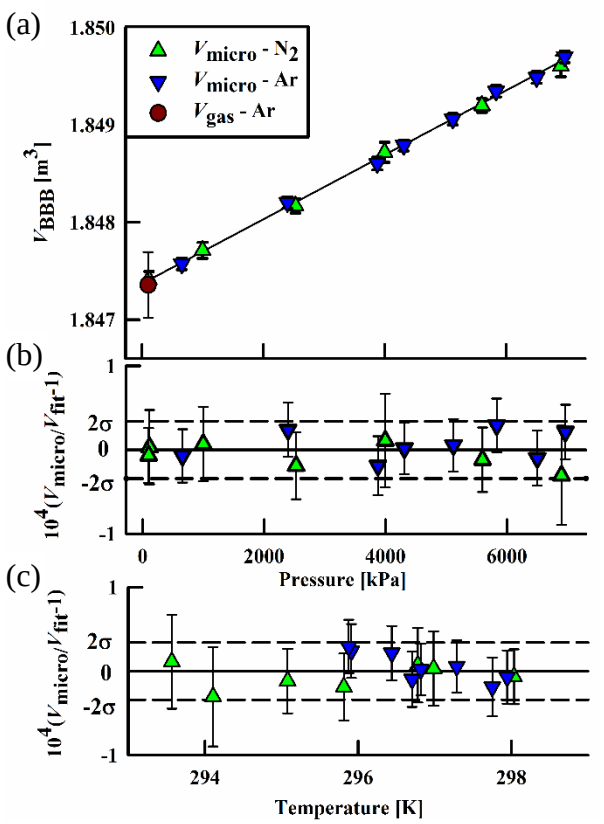

Figure 1. (a) Effect of pressure on the volume of the BBB at 295 K measured using microwaves and gas expansion. (b) fractional volume deviations from Eq. (1) as a function of pressure at 295 K, and (c) as a function of temperature at 0 MPa. The errors bars are one standard deviation of the measurements made with 3 microwave modes. The fractional standard deviation of the data from the fit was $\sigma = 17\times10^{-6}$.

Pumping gas into the BBB or bleeding gas out of the BBB is accompanied by flow work that generates temperature gradients that can be much larger than the gradients generated by fluctuations in the ambient temperature. In one test, the shell was insulated by covering it first with a layer of 2 cm-thick air-filled bubble wrap and then with a 5 mm-thick double reflective, air-filled wrap. The nitrogen pressure in the shell was raised from 0.1 MPa to 7.0 MPa in 45 minutes. Then, the top of the shell was ≈20 °C warmer than the bottom of the shell, as determined by external thermometers, as shown in Fig. 2(a). Subsequently, M_{BBB}, as computed from the average shell thermometer readings $\langle T\rangle_{\text{sh}}$ using $M_{\text{BBB}} = PV_{\text{BBB}}/(Z\langle T\rangle_{\text{sh}})$, decayed towards its final value M_∞ with a time constant $\tau \approx 5$ h, shown by the orange circles in Fig. 2(b). Here, $Z = P/(\rho RT)$ is the compressibility factor from REFPROP [5]. For the same test, M_{acoust} from Eq. (4), approached its final value with a time constant $\tau \approx 1.5$ h (the blue triangles in Fig. 2(b)). In a second, more-realistic test, the shell was not insulated and the pressure in the shell was raised from 6.6 MPa to 6.9 MPa. In this case, $PV_{\text{BBB}}/(Z\langle T\rangle_{\text{sh}})$ approached equilibrium with $\tau \approx 1.8$ h; for M_{acoust}, $\tau \approx 0.8$ h. The more-rapid equilibration of M_{acoust} is a distinct advantage of the acoustic method of determining M_{BBB}.

In deriving Eq. (3), we assumed that the gas was isothermal or, equivalently, $\rho(P, w)$ was constant throughout the cavity. When temperature gradients are present, $\rho(P, w)$ is a function of position within the cavity. Then, for Eqs. (3) and (4) to remain valid, we must replace ρ with $\langle\rho\rangle$ and $1/w^2$ with $\langle 1/w^2\rangle$, where the angled brackets indicate averages over the cavity's volume. In Section 4.2 below, we argue that $1/w^2$, as determined by Eq. (2) is a good

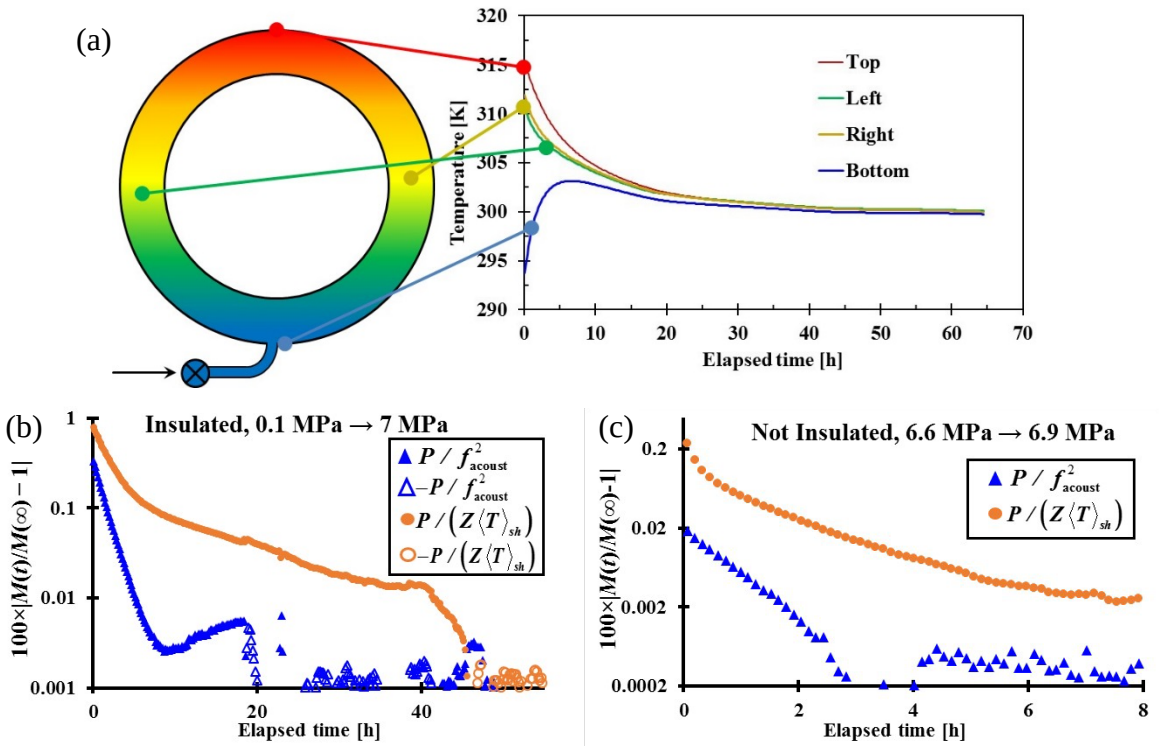

Figure 2. (a) Temperature differences on the outside of the BBB following pressurizing from 100 kPa to 7 MPa. (b) Approach to equilibrium of $P / f_{\mathrm{acoust}}^2$ and $P / \left(Z \langle T \rangle_{\mathrm{sh}}\right)$, where $\langle T \rangle_{\mathrm{sh}}$ is the average of the 4 temperature sensors shown in (a). (c) Similar to (b) following a smaller pressure change and without insulation surrounding the BBB. Note: negative values of the ordinate are plotted as open symbols.

approximation of $\langle 1/ w^2 \rangle$. Indeed, for plausible temperature distributions, the error of this approximation is on the order of $(\Delta T/T)^2$, where ΔT is a typical temperature difference in the cavity. (For ΔT = 3 K and T = 300 K, the fractional error is of order 10^{-4}).

By using the BBB as a gas collection vessel, [2] we have scaled up our experience in characterizing collection vessels by a factor of almost 10 in pressure, from 0.6 MPa to 7 MPa, and by a factor of 6 in volume, from 300 liters to 1800 liters [6]. The present work is an interim step towards gas-flow measurements traced to standards of frequency and pressure, and to the literature of $\rho(P, w)$ data. This contrasts with NIST's existing gas-flow measurements traced standards of temperature and pressure and to the literature of $Z(P, T)$ data. If this work is successful, it will shorten the scale-up chain and improve equity in large-scale natural gas transactions.

In a future publication, we will compare M_{acoust} with the M_{grav}, the mass of gas in the BBB determined by a weighing (gravimetric) technique. Our preliminary results indicate that $|M_{\mathrm{acoust}}/M_{\mathrm{grav}} - 1| < 5 \times 10^{-4}$.

The remainder of this paper is organized as follows: Section 2 describes the BBB; Section 3 describes how the volume was determined; Section 4 explains the advantages of using acoustic resonance frequencies versus thermistors for temperature measurements and describes how the average temperature is determined using radial acoustic modes; and Section 5 is the discussion.

(a) (b)

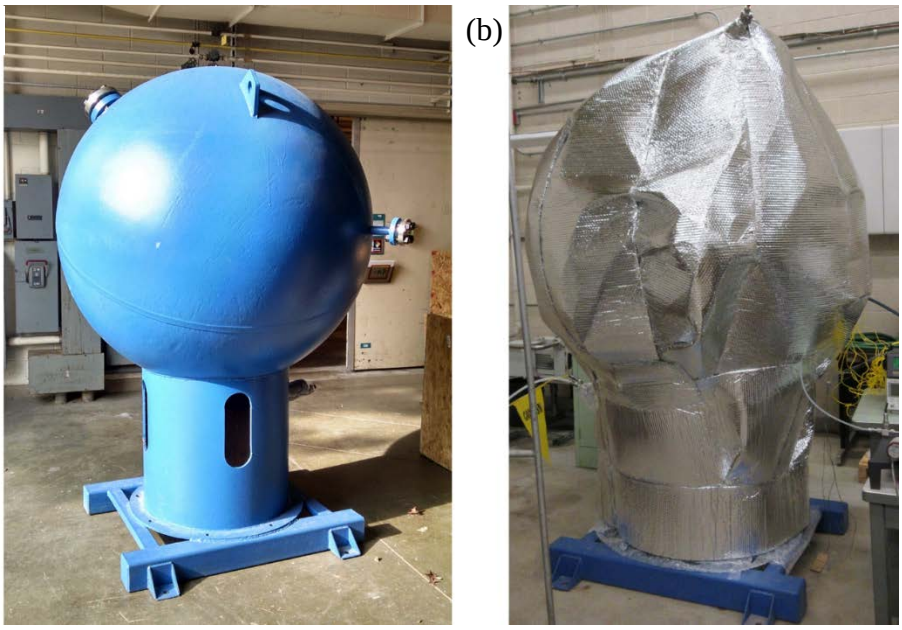

Figure 3. The BBB uninsulated (a) and insulated (b) for gas expansion experiments.

2. BBB description

The BBB was a 1.5 m diameter, nearly-spherical shell made of carbon steel of unknown composition. It had a nominal mass of 1222 kg including a welded metal pallet. See Fig. 3(a). In Fig. 3(b), the BBB is wrapped with an insulating blanket that was used during gas expansion measurements (Section 3). Table 1 lists the properties of the BBB. We believe that the BBB was manufactured in the early 1970's. Before NIST acquired the BBB, it had been stored outdoors for years. During storage, the shell's ports were open; at times the shell contained rainwater. We prepared the BBB by sandblasting and painting the exterior and by hydrostatically testing it to 9.7 MPa. To clean the BBB's interior, we poured methanol through the ports and removed it through the drain pipe. This rinsing was repeated until the drained liquid ran clear. Then, we dried the BBB by evacuating it (< 100 Pa) for 4 days. We determined the BBB's pressure-dependent internal volume while it was filled with argon. As the argon was removed from the BBB, we measured its dew point. The dew point corresponded to a water mole fraction $x_w < 4\times10^{-5}$, which had negligible effects[2] on our measurements. When the BBB was initially sealed for gas expansion experiments, the fractional leak rate, as determined from acoustic measurements [7], was approximately $(1/M_{BBB})(dM_{BBB}/dt) = -4.9\times10^{-5}$/h; we corrected our data for this leak.

The BBB had 5 small volumes (addenda) that were always connected to the spherical cavity. The addenda included 3 flanged ports and short tubes connecting each port to its flange. The addenda also included the plumbing components that permanently connected a pressure sensor to the un-flanged port. The drain tube led to a valve that was always closed. Table 2 lists the volume associated with each port, the drain, and the pressure sensor. The total volume of these addenda $V_{addenda} = 965\ cm^3 = 5.2\times10^{-4}\ V_{BBB}$. As discussed in Section 3.2, $V_{addenda}$ is not detected by the long-wavelength microwaves and sound waves used in these measurements. Therefore, our comparisons of the gas-expansion and microwave volume determinations (shown in Fig. 1) compare $(V_{gas} - V_{addenda})$ to V_{micro}.

Table 1. Properties of the BBB

Material	carbon steel
Mass	1222 kg
Inner Diameter	1.5 m
Wall Thickness	19 mm
Volume	1.8 m³
Hydrostatic Test	9.7 MPa
Working Pressure	7 MPa
Operating Temperatures	–40 °C to 49 °C

The diameter of the largest port was only 5 cm; therefore, an unaided visual inspection of the inside surfaces

[2]Adding water vapor at $x_w = 4\times10^{-5}$ to argon will increase the square of the speed of sound by the fraction 8.9×10^{-7} and, at 5 MPa, increases the dielectric constant by approximately 2.1×10^{-5}.

was uninformative. We used an articulating-head borescope to inspect the internal surfaces. To estimate the dimensions of objects in borescope images, we attached a probe (8 mm long and 5 mm wide) to the head of the borescope. Rust and other debris remained inside the BBB after it was rinsed and dried. The images showed the *rough* walls and the circumferential weld, which was approximately 2 cm wide and raised approximately 6 mm from the internal surface. The lip of the weld contained a layer of rust dust of varying thickness that could not be washed away. Despite these defects, we used microwaves to measure the volume of the BBB and used acoustic waves to measure the average gas temperature with sufficient accuracy for the present purposes. We speculate that improved accuracy could be obtained using a cleaner pressure vessel.

Table 2. Volumes of addenda measured by the gas expansion method but not by the microwave method.

Component	Volume [cm^3]	Volume/V_{BBB}
2.5 cm diameter drain tube	409	2.2×10^{-4}
P_{BBB} sensor plumbing	63	3.4×10^{-5}
5 cm diameter port	396	2.1×10^{-4}
2.5 cm diameter port	77	4.2×10^{-5}
1.3 cm diameter port	20	1.1×10^{-5}
TOTAL	965	5.2×10^{-4}

3. Volume determination

3.1 Gas expansion

We measured the internal volume of the BBB by applying the same mass-conserving, volume expansion principle and the same reference volume as reported in Ref. [8]. The result was:

$$V_{gas} = 1.84736\left(1 \pm 9.2\times10^{-5}\right)\ \mathrm{m}^3\ . \tag{5}$$

We expanded argon gas (99.999 % purity) from the BBB into a gravimetrically-calibrated, precisely-thermostated [short term: ±1 mK; $u(T)$ = 6 mK] reference volume located in a laboratory where the temperature varied from 295.3 K to 296.5 K. The final pressures in the BBB after expansions ranged from 35.67 kPa to 93.13 kPa.

Figure 4 is a schematic of the experimental set-up. A 1.27 cm-diameter tube connected the BBB's drain to the reference volume. The internal volume of this tube (1538 cm^3) was designated "$V_{inventory}$". In Fig. 4, the components of $V_{addenda}$ and $V_{inventory}$ are enclosed by a dashed curve; these components were all outside of the thermostated water bath. Initially, the reference and inventory volumes (V_{ref} + $V_{inventory}$) were evacuated to a pressure less than 1 kPa while (V_{BBB} + $V_{addenda}$) was filled with argon to 126 kPa. After thermal equilibration, the initial temperatures and pressures were recorded. Then, the valve on the BBB's drain was opened to expand the argon from (V_{BBB} + $V_{addenda}$) into (V_{ref} + $V_{inventory}$). After equilibration (typically ≈15 minutes), final temperature and pressure measurements were made. The expansion was repeated 4 times, each time by closing the valve on the BBB's drain and evacuating (V_{ref} + $V_{inventory}$) and then opening the valve to expand the argon from (V_{BBB} + $V_{addenda}$) into the evacuated volumes. After 4 expansions, the final pressure was 35 kPa. This sequence of 4 expansions was performed 3 times. A fourth experiment was performed where V_{ref} was pressurized to 128 kPa and $V_{inventory}$ and V_{BBB} evacuated to a pressure < 1 kPa and the expansion was reversed. The mutual agreement of all four sets of expansions is shown in Fig. 6.

In separate measurements, we determined $V_{inventory}$ using the same mass-conserving, gas-expansion principle. The reference volume V_{ref} was filled with argon to 130 kPa while $V_{inventory}$ was evacuated to a pressure less than 1 kPa. The expansion of the argon from V_{ref} into $V_{inventory}$ yielded the result $V_{inventory}$ = (1358 ± 25) cm³, where the uncertainty is one standard uncertainty.

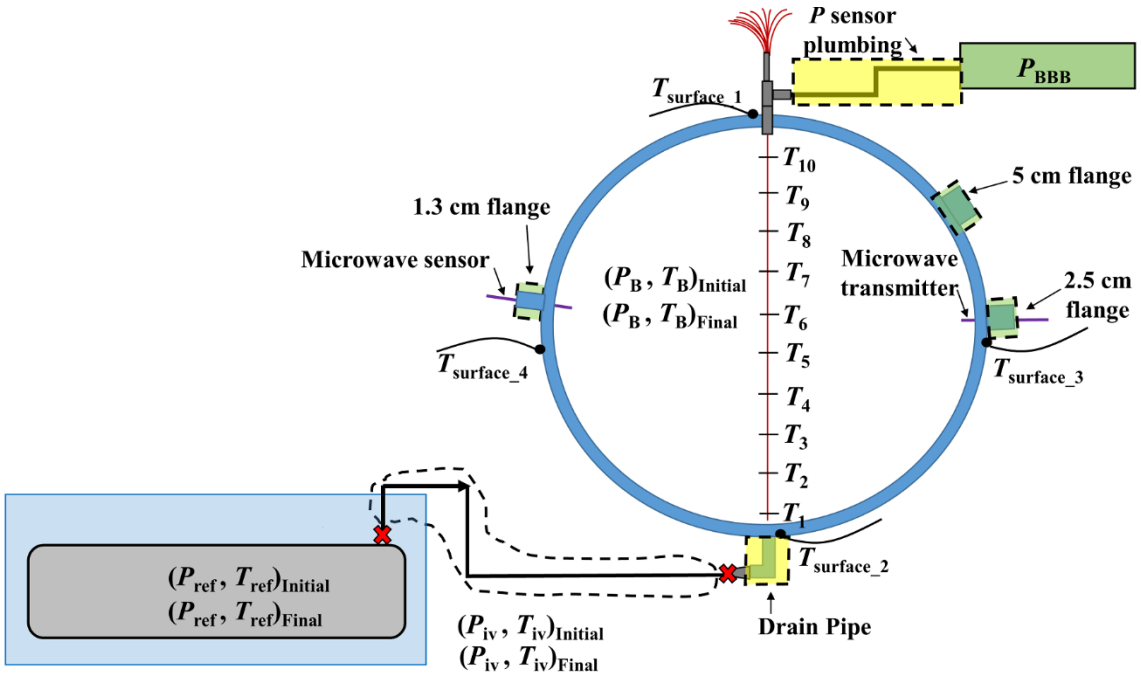

Figure 4. Schematic of BBB gas expansion set-up showing the extra plumbing that the gas expansion method measures but is excluded from the microwave measurements. The subscripts "iv", "ref", and "B" denotes inventory volume, the reference volume and the BBB volume, respectively.

The gas expansion method requires an accurate estimate of the volume-averaged density of the argon in the BBB preceding and following each expansion. This estimate requires a model for the temperature distribution in the argon. The largest uncertainty component of V_{gas} results from the uncertainty of the temperature distribution. Temperature fluctuations in the laboratory, combined with limited air circulation, generated time-dependent temperature gradients in the BBB. (The BBB was too large to fit in the thermostated laboratory with the reference volume.)

Figure 7(b) displays a typical, approximately-linear, vertical, temperature profile in the argon inside the BBB; the top was 0.4 K warmer than the bottom. We determined the volume-averaged temperature[3] using 10 thermocouples, equally-spaced along the vertical diameter of the BBB and by 4 surface thermistors placed equal-distant along the vertical and horizontal axis. (See Fig. 4.) Before insulating the BBB, the temperature uncertainty contributed more than 88 % of the density-change uncertainty. Insulating the BBB decreased the temperature difference between the top and bottom by nearly a factor of 2 and reduced the relative uncertainty of V_{gas} from 0.030 % to 0.019 % (k = 1).

3.2 Microwave measurements

We made an independent determination of the BBB volume by measuring the frequencies of microwave resonances. This technique is described in more detail in Ref. [8]. To measure the microwave resonance frequencies, we installed transmitting and receiving antennas into two of the ports in the BBB (see Fig. 5). One microwave (MW) antenna was installed into the 1.3 cm-diameter port, as shown Fig. 5(b). The other MW antenna was installed along with a sound source (speaker) into the 5 cm-diameter port, as shown in Fig. 5(c). Electrical connection to each antenna was made using a Bayonet Neill – Concelman (BNC) hermetic feedthrough with a 3/8" NPT fitting

[3] Technically $\langle\rho\rangle$ requires the determination of $\langle 1/T\rangle$ not $1/\langle T\rangle$. However, the fractional difference between the two averages is $(\sigma/\langle T\rangle)^2 \approx 10^{-4}$ to lowest order, where σ is the standard deviation of the temperatures.

mounted into the port flange. The MW antennas were made from semi-rigid coaxial cable with solid copper shield, polytetrafluoroethylene insulation, and silver-plated, solid copper center conductor. As shown in Figs. 5(b) and 5(c), the shield and insulation of the coaxial cables extended from the electrical feedthroughs along the lengths of ports to the inside surface of the BBB. About 2 cm from the opening into the BBB, the coax passed through a small hole in a coarse mesh copper screen and was secured to it with soft solder. The screen performed 3 functions: 1) it rigidly held the coax centered in the duct, 2) it grounded the shield to the metal shell, and 3) it prevented the penetration of microwaves into the duct, yet it allowed gas and sound waves to freely pass. The bare center conductor extended 11 cm further into the BBB forming a straight antenna that coupled to the electric field. The antenna protruded into the BBB by 14 % of the BBB's radius, the same length-to-radius ratio used in Ref [8]. Following Ref. [8], we estimate the protruding center conductors shifted the microwave resonance frequencies by the fraction 2×10^{-5} or less. The antenna in the 1.3 cm-diameter port had a 1 cm-diameter loop to improve coupling to the magnetic field.

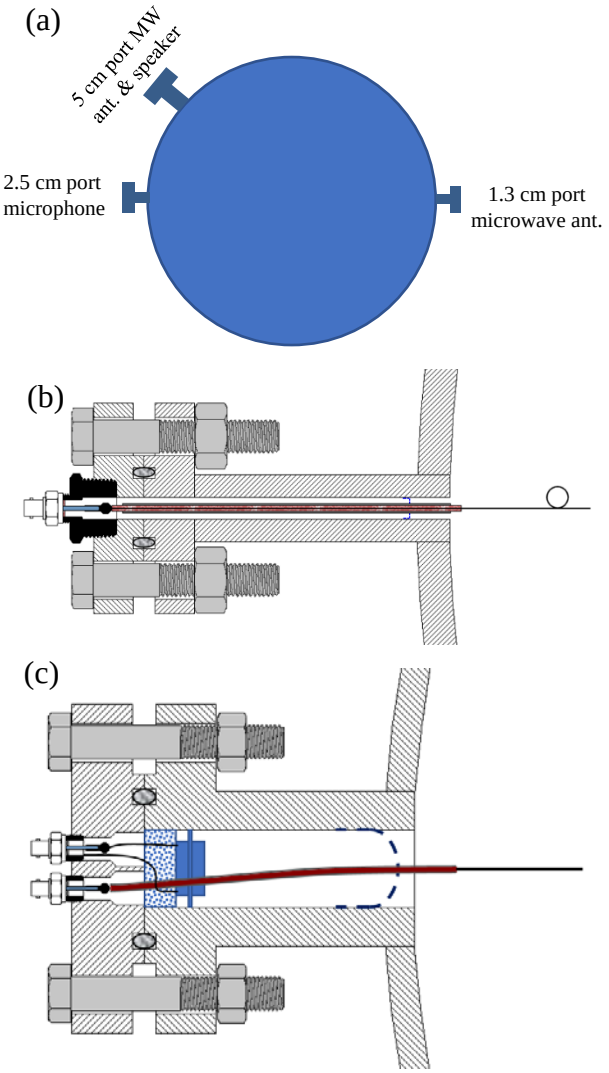

Figure 5. (a) Port locations and uses. (b) Microwave (MW) antenna mounted in the 1.3 cm-diameter port. (c) MW antenna and a 38 mm-diameter loudspeaker (dark blue rectangle) mounted in the 5-cm diameter port. Flexible foam material dampened the sound emitted from the rear of the speaker.

The theory for the electromagnetic modes of a spherical cavity is described in detail in Refs. [9] and [10]. Following conventional derivations in the literature, we divide the modes into two types: transverse electric (TE) and transverse magnetic (TM) modes, according to which field (electric or magnetic, respectively) has its radial component identically equal to zero. Modes are designated TE*ln* and TM*ln*, where *l* and *n* are integers greater than zero that identify the eigenfunction and the resonance frequency f_{ln}^{σ} (with σ = TE or TM). In a perfectly spherical chamber, the resonance frequencies form (2*l*+1)-fold degenerate multiplets; however, the degeneracy may be partially or fully lifted by perturbations in the shape, such as imperfect sphericity or the existence of ports. The resonance frequencies of a gas-filled spherical cavity with radius *a* and a rigid, perfectly conducting wall are given by

$$f_{ln}^{\sigma} = \frac{\xi_{ln}^{\sigma} c_0}{2\pi n_g a} \quad , \tag{6}$$

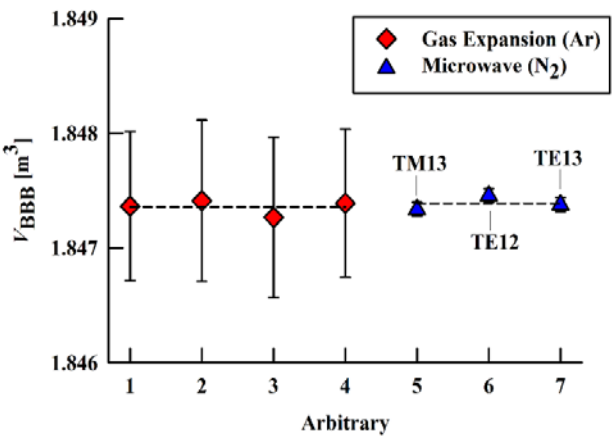

Figure 6. Comparison of the volume of the BBB at 100 kPa and 295 K as determined by gas expansion using argon gas and microwave measurements using nitrogen gas.

where ξ_{ln}^{σ} is an exactly known eigenvalue, c_0 is the speed of light in vacuum, and n_g is the refractive index of the gas. If the resonance frequency is measured and $n_g(T, P)$ is known, then Eq. (6) can be inverted to determine $a(T, P)$. When the degeneracy is lifted by shape perturbations, Eq. (6) still holds to first order if f_{ln}^{σ} is replaced by the average frequency of the multiplet $\left\langle f_{ln}^{\sigma} \right\rangle$ [9]. When the perturbation is small, the multiplet will be partially resolved, and a precise determination of $\left\langle f_{ln}^{\sigma} \right\rangle$ will be difficult if the multiplicity is large. Therefore, we focus on the modes with the lowest multiplicity, the $l = 1$ triplets.

We used a commercially-manufactured, microwave network analyzer to measure the electromagnetic power transmitted from one antenna through the BBB to the other antenna as a function of frequency. The measurements were conducted while the BBB was filled with high purity nitrogen or argon. We measured the complex response (the parameter S12) in the vicinity of 3 modes TM13, TE12, and TE13. Because each mode was a triplet that was not fully resolved, we fitted the data with a function that was the complex sum of 3 resonances plus a complex background, as described in Ref. [10]. The 3 peak frequencies for the resonances in the triplet, resulting from the fit, were averaged to determine the inner radius a of the BBB using the relation:

$$a = \frac{\xi_{1n}^{\sigma} c_0}{2\pi n_g \left\langle f_{1n}^{\sigma} \right\rangle} . \tag{7}$$

The refractive index $n_g(T, P)$ of the gas was obtained from Ref. [5]. The volume at 100 kPa and 295 K determined from the 3 microwave modes is

$$V_{\text{micro}} = 1.84743\left(1 \pm 1.1 \times 10^{-4}\right) \text{ m}^3 . \tag{8}$$

Equation (8) includes type A (random) and type B (systematic) uncertainties. The type B uncertainty is the standard deviation of the volume determined from 5 microwave modes (TM12, TM13, TE11, TE12, and TE13) and is an estimate of the effects of perturbations, such as non-sphericity and surface roughness, that are not included in our model of the microwave modes in the BBB. Figure 6 shows the agreement between V_{micro} and V_{gas} at 100 kPa and 295 K, $V_{\text{micro}}/V_{\text{gas}} - 1 = (2 \pm 14) \times 10^{-5}$.

We measured $V_{\text{BBB}}(P, T)$, the volume of the BBB as a function of temperature and pressure. The results are plotted in Fig. 1 and summarized by the fit in Eq. (1). The microwave measurements in nitrogen and in argon spanned the pressure range 100 kPa to 7 MPa and spanned laboratory temperatures between 293 K and 298 K. Equation (1) is valid over the rated working pressure range of the BBB. We expect, but cannot guarantee, the validity of Eq. (1) outside the measurement temperature range.

4. Estimating the average temperature

4.1 Temperature sensor array

For a traditional *PVTt* primary gas flow standard, any errors in the gas temperature are directly transferred into errors in the calculated mass. The average temperature of the collected gas is difficult to measure, especially in un-thermostated environments. When pressurized gas flows into a large tank, the flow generates different temperatures in different parts of the tank. When the inflow stops, buoyancy-driven convection moves the warmest gas to the top of the tank and the coolest gas to the bottom. This stratification makes it difficult to measure the average temperature by conventional means. A prompt reading of a few thermometers is inherently inaccurate, and temperature gradients persist within the stagnant gas in big tanks.

As discussed in Section 3, during the gas expansion experiments, the BBB was instrumented with an internal thermocouple array consisting of ten thermocouples

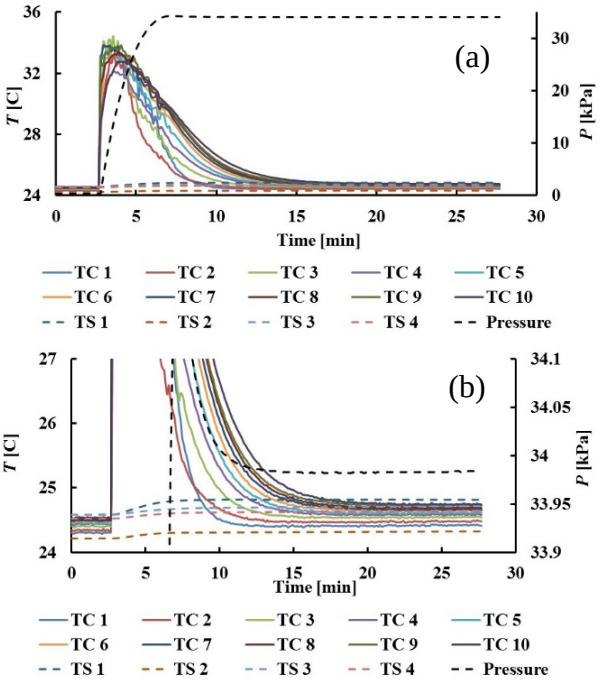

Figure 8. (a) Temperature and pressure profile inside the BBB. The solid lines are measurements from the internal thermocouple (TC) array and the dashed lines are the temperature measured by the surface thermistors (TS). (b) Expanded view of (a).

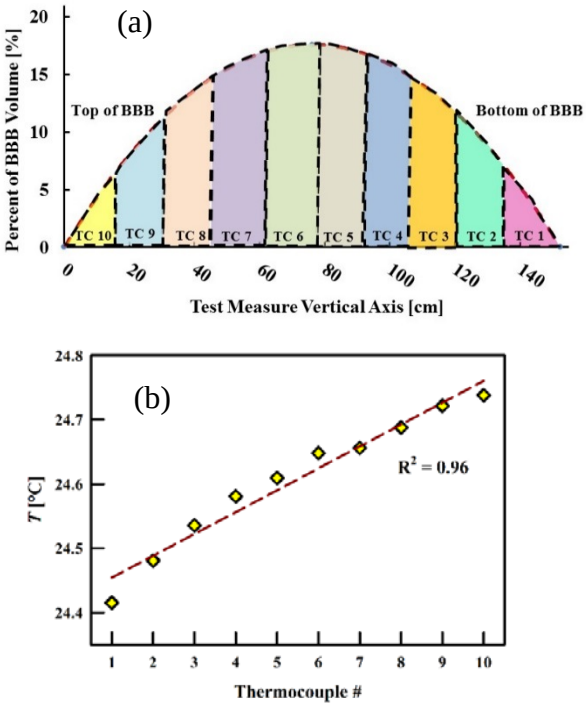

Figure 7. (a) Graphical representation of how thermocouple measurements are volume weighted. (b) Linear temperature distribution with respect to height in the BBB.

spaced at approximately 15.25 cm vertical intervals extending from the top of the BBB to its bottom. In addition, 4 surface thermistors were located at the top, the bottom, and on opposite sides of the equator of the BBB. We averaged the temperatures determined by the internal thermocouple array, weighting each thermocouple by the fractional volume of the BBB at its height. Figure 7(a) illustrates the volume weighting for a half sphere. Figure 7(b) shows the stratified temperature distribution for a quiescent state in the BBB while it was insulated. Usually, the temperature distribution in the BBB was a linear function of the height whether or not the BBB was insulated. When uninsulated, the quiescent temperature distribution spanned a larger temperature range (typically 1 K), reflecting the temperature distribution in the room.

The thermocouple array is advantageous because it captures the "fast" temperature transients in the BBB, whereas the surface thermistors do not. Figure 8 shows

the temperature profile in the BBB measured by the thermocouple array and the surface thermistors after pressurizing from < 1 kPa to approximately 30 kPa in less than 3 minutes.

The equilibration in Fig. 8 is roughly consistent with a simple model that ignores convective heat transfer. We consider the thermal equilibration of a spherical substance with radius a by radial heat conduction only [11]. The slowest time constant characterizing equilibration is $\tau = a^2/(D_T \pi^2)$, where D_T is the thermal diffusivity of the sphere. For argon at 295 K, $D_T \approx (0.7\ \mathrm{cm^2/s}) \times (P/30\ \mathrm{kPa})$ [5]. This model predicts $\tau \approx 14$ min for 30 kPa, which is approximately what we observed.

At 30 kPa, the surface thermistors did not capture the "fast" temperature transient generated by pressurizing the BBB; however, they did agree (within 80 mK) with the volume weighted average of the internal thermocouples after ≈20 minutes had passed. In these experiments, the BBB was insulated. However, the insulation was removed in subsequent experiments allowing the internal gas to more quickly equilibrate with the room. Remaining questions are: 1) how long does it take for the temperature to equilibrate following more extreme pressure changes? and 2) how accurate are the surface thermistors when the pressure and mass of gas in the BBB are two orders of magnitude larger than the conditions in Fig. 8 and the BBB is not insulated? For a *PVTt* primary standard to be practical, the thermal equilibration time and the accuracy of the temperature measurement must be acceptable. To answer these questions, we relied on the surface thermistors and measured acoustic resonance frequencies. We could not use the internal thermocouple array because the wires leading to the thermocouples interfered with the microwave measurements.

As discussed in Section 1 and shown in Fig. 2, the mass of gas deduced from the acoustic resonance frequencies and the internal gas pressure $M_{\mathrm{acoust}} \propto (P / f_{\mathrm{acoust}}^2)$ equilibrated significantly faster than the mass determined by the pressure and the average surface thermistor reading $P/(Z\langle T\rangle_{\mathrm{sh}})$. Furthermore, the masses determined by these methods long after a pressure change (at time infinity, M_∞) are inconsistent by as much as 0.25 % because the temperature in the laboratory is not controlled and changes in a diurnal cycle. (There is always at least a small discrepancy between the shell temperature and the internal gas temperature.) In the example in Fig. 2, M_{acoust} was determined within a 0.01 % uncertainty 8-times faster than the mass determined from the surface thermistors using $P/(Z\langle T\rangle_{\mathrm{sh}})$.

At this time, we have not completed reference measurements that validate M_{acoust}. In a future publication, we will report results utilizing a weighing rig to transfer 20 kg aliquots of argon into the BBB. Preliminary results indicate that $|M_{\mathrm{acoust}}/M_{\mathrm{grav}} - 1| < 5\times10^{-4}$.

4.2 Acoustic resonance frequency

Figure 5(a) shows the positions of the acoustic transducers in the BBB. The sound source, a voice-coil speaker with a hard-plastic cone, was mounted in the 5 cm-diameter port (Fig. 5(c)). A flexible foam material was placed behind the speaker to dampen the sound emitted from the rear of the speaker. The detector transducer (microphone) was mounted in the 2.5 cm-diameter port (Fig. 9). The detector was a 32 mm-diameter, 0.38 mm-thick, bimorph piezoceramic bending disk mounted to the flange with flexible caulk.

Previously, we have shown how the mass M of gas in a pressure vessel with volume V may be deduced from measurements of the gas pressure P and the frequencies f_{acoust} of acoustic resonances within the vessel. The mass

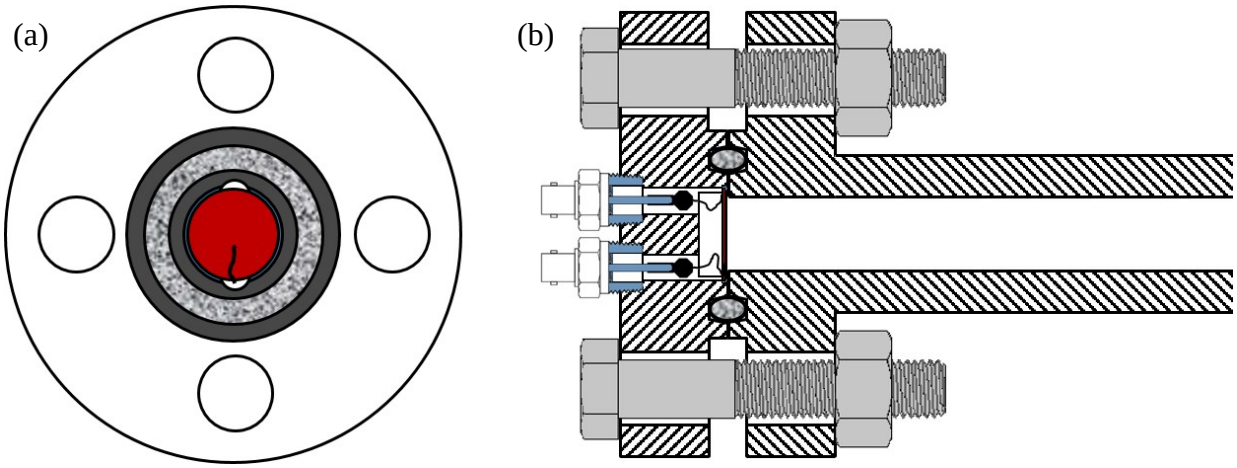

Figure 9. Schematic of the acoustic detector. (a) 32 mm diameter, 0.38 mm thick bimorph piezoceramic bending disk (red) mounted with flexible caulk in flange on the 2.5 cm diameter port. Small vents permit static pressure equilibration and connection to electrode. (b) Cross section view of assembled flanges and port duct. Two BNC, 3/8-NPT (10 MPa) feedthroughs are used for differential detection of the signal from the bimorph electrodes.

determined with this technique was shown to be insensitive to time-independent temperature gradients in the gas. The acoustic measurements eliminated the need for multiple thermometers to determine the average gas temperature with sufficient accuracy for flow metrology.

In a uniform gas, the speed of sound w is proportional to $\sqrt{T}$ plus small corrections, where T is the thermodynamic temperature of the gas. An acoustic mode of the gas in a pressure vessel is a standing wave with velocity potential $\varphi_i(\mathbf{r})$ and wavenumber k_i, where i denotes a set of indices that identify the mode; $\varphi_i(\mathbf{r})$ and k_i are gas independent. A driven sound wave in the confined gas has maximum amplitude at the resonance frequency $f_{\text{acoust}} \propto w$. The basis of acoustic gas thermometry is the inversion of the relationship to determine the gas's thermodynamic temperature from measured resonance frequencies.

When the temperature is not uniform, the speed of sound in the gas is spatially dependent. To first order, the resonance frequencies are determined by a mode-dependent, weighted average of $[w(\mathbf{r})]^2$ over the volume, where $w(\mathbf{r})$ is the local speed of sound. Thus, $f_{\text{acoust}}^2 \propto \langle w^2 \rangle_\varphi$, where [7]

$$\langle w^2 \rangle_\varphi = \frac{\int_V w(\mathbf{r})^2 |\varphi_i|^2 \, dV}{\int_V |\varphi_i|^2 \, dV} \tag{9}$$

In spherical coordinates, the volume differential $dV = r^2 dr \, d\Omega$, where $d\Omega$ is a differential solid angle. The acoustic velocity potential φ_i is proportional to the local acoustic pressure in the standing wave. Regions where $\varphi_i = 0$, *i.e.* pressure nodes, do not contribute to the weighted average. (See Fig. 10.) In effect, $\langle w^2 \rangle_\varphi$ is proportional to the mode-dependent average temperature $\langle T \rangle_\varphi$. However, the average density of the gas in the vessel is dependent on the *volume* average of $1/T$. Because typical temperature variations δT are small, we can approximate $\langle 1/T \rangle$ by $1/\langle T \rangle$ with fractional errors of order $(\sigma / \langle T \rangle)^2 \approx 10^{-4}$, where σ is the standard deviation of the temperature. The remainder of

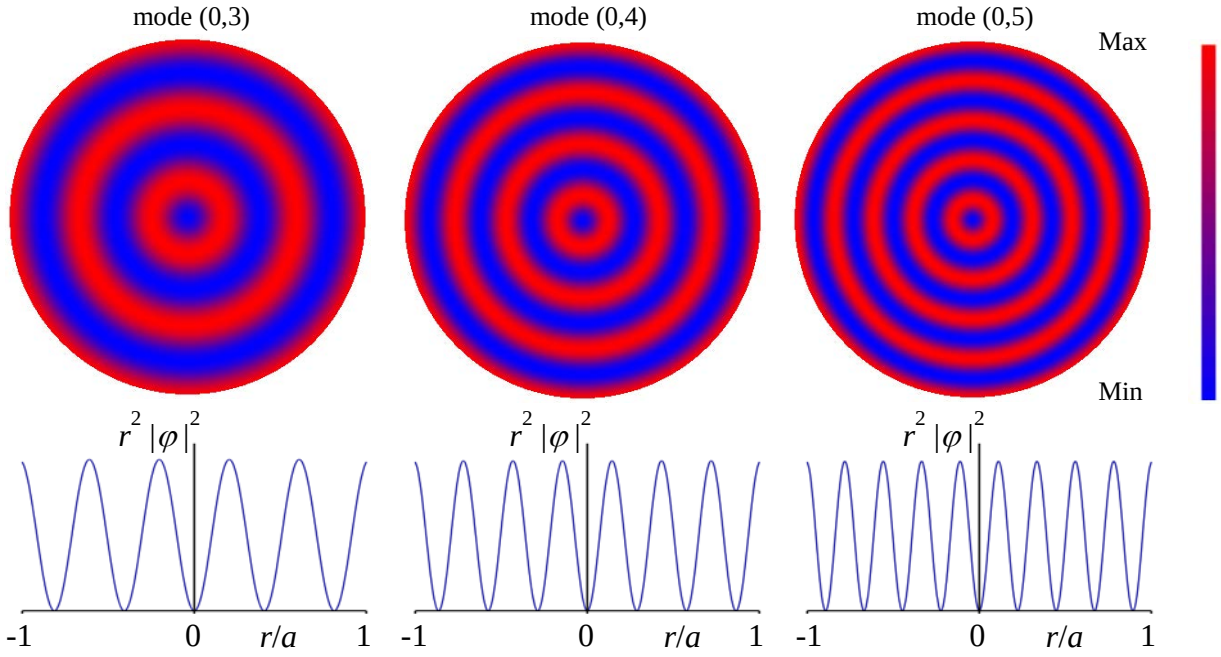

Figure 10. Top: Plots of the weighting function $r^2|\varphi|^2$ for 3 radial acoustic modes of a gas in a spherical cavity. Bottom: Graphs of $r^2|\varphi(r)|^2$ as a function of r/a. The plots are normalized by $\oint_V |\varphi|^2\, dV$ and have the same vertical scale.

this section explores the difference between $\langle T\rangle_\varphi$ and $\langle T\rangle_V \equiv (1/V)\int_V T(\mathbf{r})\, dV$ for simple temperature profiles in spherical and cylindrical pressure vessels and gives specific recommendations.

Gillis, *et al*. [6] showed that the measured resonance frequencies in a cylindrical vessel did not change to first order when a linear temperature gradient was imposed, while $\langle T\rangle_V$ was kept fixed, in agreement with first order perturbation theory, *i.e.* $\langle T\rangle_\varphi \equiv \langle T\rangle_V$ for a linear temperature gradient in a cylindrical vessel. The same is true in a spherical vessel. Figure 10 shows plots of $[r^2|\varphi(r)|^2]$ for three radial modes of a spherical cavity; the plots are normalized by the integral $\int_V |\varphi(\mathbf{r})|^2\, dV \equiv V\Lambda_\alpha$ and plotted on the same scale. (We use radial modes because they are non-degenerate and have the highest quality factors.) Because $[r^2|\varphi(r)|^2]$ is an even function about any plane through the sphere's center, a gradient in w^2 (or T) that is an odd function of the distance from that plane (*e.g.* linear) will integrate to zero in Eq. (9). Gradients that are not odd functions of the distance will, generally, have non-vanishing integrals.

During pressurization of the BBB, gas expanding past a throttle valve in the exterior plumbing cools by 20 °C or more before entering the BBB as a jet. Inside, the cold gas sinks to the lower region of the vessel, while the compressing gas heats up and rises to the top. The resulting density gradients and mass currents are too complex to model accurately. Instead, to compare the volume and mode averages, we considered the very simple step-function temperature distribution given by

$$T(z) = T_1 + \left[H(z - z_h) - 1\right]\Delta T\,, \qquad H(z - z_h) = \begin{cases} 0, & z < z_h \\ 1, & z > z_h \end{cases} \tag{10}$$

shown in Fig. 11. Here, $z_h \equiv -a + h$ is the z-coordinate for the location of the interface and $\Delta T = T_1 - T_2$. The volume-average temperature defined above becomes

$$\langle T \rangle_V = T_1 \frac{V_1}{V} + T_2 \frac{V_2}{V}, \tag{11}$$

which is a function of h. In a spherical geometry Eq. (11) becomes

$$\langle T \rangle_V = T_1 - \frac{3}{4}\frac{h^2}{a^2}\left(1 - \frac{1}{3}\frac{h}{a}\right)\Delta T\,. \tag{12}$$

The mode-average temperature obtained from Eq. (9) for the radial mode (0,n) becomes

$$\langle T \rangle_{\varphi_{0n}} = T_1 - \Delta T \int_{V_2} \frac{|\varphi_{0n}|^2}{V \Lambda_{0n}} dV \tag{13}$$

where the velocity potential is a function of r only

$$\varphi_{0n}(r) = j_0\left(\zeta_{0n}\, r/a\right), \text{ with } \Lambda_{0n} = \frac{3}{2}\left[\, j_0\left(\zeta_{0n}\right)\right]^2, \tag{14}$$

j_0 is the zeroth order spherical Bessel function, and the eigenvalue ζ_{0n} is the n^{th} root of $\zeta = \tan\zeta$. The averages $\langle\, T \,\rangle_V$ and $\langle\, T \,\rangle_\varphi$ from Eqs. (12) and (13) are plotted in Fig. 12(a) as a function of h/a for n = 2, 3, and 4. The fractional difference between these two averages is approximately

$$\frac{\langle T \rangle_{\varphi_{0n}} - \langle T \rangle_V}{\langle T \rangle_V} \approx \frac{\Delta T}{T_1}\left[\frac{3}{4}\frac{h^2}{a^2}\left(1 - \frac{1}{3}\frac{h}{a}\right) - \frac{2}{3V}\int_{V_2}\left(\frac{j_0\left(\zeta_{0n}\, r/a\right)}{j_0\left(\zeta_{0n}\right)}\right)^2 dV\right] \tag{15}$$

to first order in the small quantity $\Delta T / T_1$. For the extreme case considered in Figs. 2(a) and 2(b), ΔT = 20 K and T_1 = 300 K, $\Delta T / T_1 \approx 0.07$. For a more typical case (Fig. 2(c)) ΔT = 1.5 K and $\Delta T / T_1 \approx 0.005$ immediately after a gas collection.

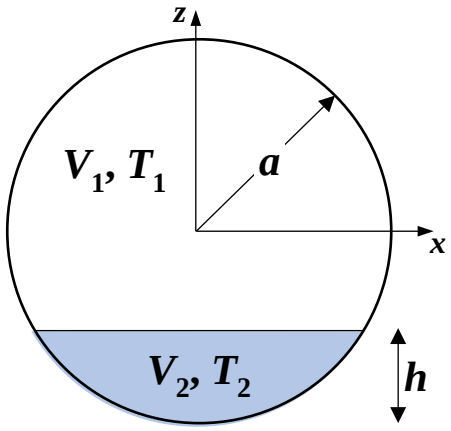

Figure 11. Simple temperature distribution in spherical vessel with radius a and volume $V = 4\pi a^3/3 = V_1 + V_2$. Upper region has volume V_1 and uniform temperature T_1; lower region with height h has volume V_2 and uniform temperature $T_2 < T_1$.

The quantity inside the square brackets in Eq. (15), which is a function only of h/a for a given radial mode n, is plotted in Fig. 12(b) for radial modes (0,n) with n = 2, 3, 4, and the limit of large n (dashed line). The central result from this simple model of temperature gradients in a spherical vessel is that the radial-mode-average $\langle w^2 \rangle_\varphi$, and therefore the density, may be in error, fractionally, by as much as $0.1 \times (\Delta T / T_1)$.

For completeness, we also investigated using non-radial modes to measure $\langle w^2 \rangle_\varphi$. Non-radial modes are identified by two integers (l,n) with $l > 0$ and have degeneracy $2l + 1$. The "simplest" non-radial mode is the (1,1) mode, and it is 3-fold degenerate. The three components of the

triplet have nodal (zero weight) planes that are mutually perpendicular and pass through the sphere's center. For one component the *xy*-plane is a nodal plane, and the greatest weight occurs in lobes above and below the nodal plane. Thus, this component will be most sensitive to gradients in the *z*-direction. The other two components have the *xz* and *yz*-planes as nodal planes. These components will do a better job of averaging over the gradient. Unfortunately, the acoustic microphone and source do not couple to the three components with equal efficiency, and there is no easy way to determine what average over these components is appropriate. For these and other reasons, we have chosen to measure the frequencies of only the (non-degenerate) radial modes.

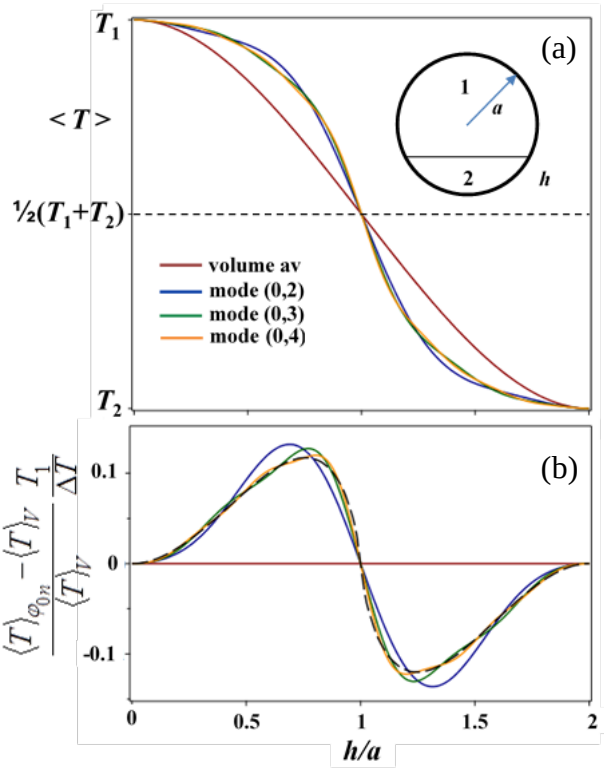

Figure 12. (a) The averages $\langle T \rangle_V$ and $\langle T \rangle_\varphi$ in a gas-filled spherical vessel from Eqs. (12) and (13) for n = 2, 3, and 4. (b) Scaled fractional difference between the volume and mode averages from Eq. (15). The black dashed curve is the large n limit.

We also investigated this model for a cylindrical geometry. For a cylindrical vessel, we need to consider the orientation of the cylinder's axis relative to the gradients that are likely to develop in earth's gravity, *i.e.* the gradient is a function of *z* only. For the reasons discussed above, we looked only at non-degenerate modes of the gas-filled cylindrical vessel, *i.e.* longitudinal and transverse radial modes, to determine $\langle w^2 \rangle_\varphi$. For a horizontal cylinder, the temperature gradient is perpendicular to the cylinder axis. $|\varphi(\mathbf{r})|^2$ for the longitudinal modes is only a function of the axial coordinate, so the temperature in V_1 and V_2 will be given equal weight. Therefore, the volume-average and longitudinal mode-average will be the same. Radial mode averages for a horizontal cylinder could be in error by as much as $0.1\times(\Delta T / T_1)$, similar to radial modes in spheres.

For vertically oriented cylindrical vessels, *i.e.* the gradient is parallel to the cylinder axis, the situation is reversed: $|\varphi(\mathbf{r})|^2$ for the radial modes is only a function of the coordinates perpendicular to the gradient, so the mode average is the same as the volume average. Longitudinal modes (parallel with the gradient) have averaging errors that diminish as $1/(2\pi l)$, where l is the longitudinal mode number. Table 3 summarizes the results of the linear and step temperature distributions.

Table 3. Fractional difference between $\langle T \rangle_V$ and $\langle T \rangle_\varphi$ for a linear gradient (dT/dz = constant) and the step function defined in Eq. (10) (Fig. 11). Results from first-order perturbation theory are given for a spherical resonator (radial modes) and a cylindrical resonator oriented horizontally or vertically using longitudinal and radial modes.

	Temperature Distribution	Spherical resonator	Cylindrical vessel	
			axis horizontal	axis vertical
linear	$T(z) = T_0 + (dT/dz)\, z$	0 (radial)	0 (longitudinal)	0 (radial)
step	$T(z) = T_1 + [H(z-z_h)-1]\,\Delta T$	$< 0.1\ (\Delta T/T_1)$ (radial)	$< 0.1\ (\Delta T/T_1)$ (radial)	0 (radial)
			0 (longitudinal)	$< (\Delta T/T_1)/2\pi l$ (long.)

5. Discussion

We characterized a 1.8 m^3, nearly-spherical, steel shell at pressures up to 7 MPa for use as a collection vessel or source for gas flow standard. We measured the cavity's microwave resonance frequencies f_{micro} to determine its pressure- and temperature-dependent volume: $V_{micro}(P, T) = 1.84740\ m^3 \times [1 + \alpha(T - 295\ K) + \kappa P]$ with a fractional uncertainty of 0.011 % at a 68 % confidence level. The coefficients α and κ were consistent with the dimensions and properties of the steel shell. The microwave-determined volume V_{micro} was consistent, within combined uncertainties, with V_{gas} the volume determined by a gas expansion method: $V_{micro}/V_{gas} - 1 = (2 \pm 14)\times10^{-5}$.

When the shell was filled with gas, measurements of its acoustic resonance frequencies f_{acoust} and of the pressure quickly and accurately determined the mass of the gas in the shell, even when temperature gradients persisted. We have shown that despite the large thermal gradients that develop when gas is added or removed from the BBB, the mass M_{acoust} of gas determined from acoustic resonance frequencies settled to within 0.01 % of its final value much faster than the estimated mass determined from the shell temperature. Following a pressure change of 0.3 MPa, the top-to-bottom temperature difference was 1.5 °C and M_{acoust} settled to its final value in just 0.5 h. Proportionately longer times were required after larger pressure changes generated larger temperature differences. In a subsequent publication, we will compare the mass M_{acoust} of gas in the BBB determined from acoustic measurements with M_{grav} determined gravimetrically. This comparison will determine the accuracy with which we can measure the mass of gas from acoustic measurements. Our preliminary measurements indicate $|M_{acoust}/M_{grav} - 1| < 5\times10^{-4}$.

Finally, based on our study of acoustic measurements in collection vessels with vertical temperature gradients, cylindrical vessels may have advantages over spherical vessels. Measurements of $\langle w^2 \rangle$ and, therefore, $\langle \rho \rangle$ from the longitudinal acoustic modes of a gas-filled, horizontal cylindrical vessel should be insensitive to vertical temperature gradients, contributing an uncertainty to the mass of order $(\Delta T/T)^2$. For a vertical cylinder, the uncertainty due to vertical temperature gradients using longitudinal modes are first order in $(\Delta T/T)$, but decrease as the mode order increases. The uncertainty for radial acoustic modes in a vertical cylindrical vessel should be second order.

6. References

[1] A.N. Johnson. "Natural Gas Flow Calibration Service" NIST special publication 1081, August 2008.

[2] J.D. Wright, A.N. Johnson, M.R. Moldover, and G.M. Kline "Gas Flowmeter Calibrations with the 34 L and 677 L *PVTt* Standards" NIST Special Publication 250-63, November 2010.

[3] A.N. Johnson, C. Li, J.D. Wright, G.M. Kline, and C.J. Crowley. "Improved Nozzle Manifold for Gas Flow Calibrations", 8th International Symposium on Fluid Flow Measurement. Colorado Springs, CO, U.S.; 6/18/2012 to 6/22/2012.

[4] J.P.M. Trusler, *Physical Acoustics and Metrology of Fluids* (Adam Hilger, Bristol, 1991).

[5] E.W. Lemmon, M.O. McLinden, and M.L. Huber, "REFPROP: Reference Fluid Thermodynamic and Transport Properties," NIST Standard Reference Database 23, Version 9.1, Natl. Inst. Stand. and Tech., Boulder, CO, (2010) www.nist.gov/srd/nist23.cfm

[6] K.A. Gillis, J.B. Mehl, J.W. Schmidt, and M.R. Moldover. "'Weighing' a gas with microwave and acoustic resonances", Metrologia. **52**, 337-352 (2015).

[7] K.A. Gillis, M.R. Moldover, and J.B. Mehl, "Detecting Leaks in Gas-Filled Pressure Vessels Using Acoustic Resonances", Rev. Scientific Instrum. **87**, 054901 (2016).

[8] M.R. Moldover, J.W. Schmidt, K.A. Gillis, J.B. Mehl, and J.D. Wright. "Microwave determination of the volume of a pressure vessel", Meas. Sci. Technol. **26**, 015304 (2015).

[9] J.B. Mehl and M.R. Moldover, "Measurement of the ratio of the speed of sound to the speed of light," Phys. Rev. A **34**, 3341-3344 (1986).

[10] E.F. May, L. Pitre, J.B. Mehl, M.R. Moldover, and J.W. Schmidt, "Quasi-spherical cavity resonators for metrology based on the relative dielectric permittivity of gases," Rev. Sci. Instrum. **75**, 3307-3317 (2004).

[11] H. S. Carslaw and J. C. Jaeger, *Conduction of Heat in Solids: 2nd Edition* (Clarendon Press, Oxford, Great Britain, 1959), Section 9.3.